Int. J. Electrochem. Sci., 6 **(2011)** 3483 - 3496

International Journal of
ELECTROCHEMICAL
SCIENCE
www.electrochemsci.org

The Effect of Temperature on the Electrochemical Behavior of the V(IV)/V(V) Couple on a Graphite Electrode

Liu Hui-jun[1], *Xu Qian*[1,*], *Yan Chuan-wei*[2], *Cao Ya-zhe*[1], *Qiao Yong-lian*[1]

[1] School of Materials Science and Metallurgy, Northeastern University, Shenyang,110819, P R China.
[2] State Key Laboratory for Corrosion and Protection, Institute of Metal Research, Chinese Academy of Sciences, Shenyang 110016, P R China.
[*]E-mail: qianxu201@mail.neu.edu.cn

Received: 29 May 2011 / *Accepted:* 5 July 2011 / *Published:* 1 August 2011

The electrochemical behavior of the V(IV)/V(V) couple in an aqueous solution of 2 mol dm^{-3} H_2SO_4+2 mol dm^{-3} $VOSO_4$ on a graphite electrode at different temperatures is studied by steady-state polarization and electrochemical impedance spectroscopy. The results show that the diffusion coefficient (*D*) of V(IV) species increases from 1.60×10^{-5} to 3.15×10^{-5} cm^2 s^{-1} with temperature from 15 to 70 ^oC and the activation energy for diffusion of V(IV) species is 10.52 kJ mol^{-1}. The anodic oxidation of V(IV) is a mixed kinetic-diffusion controlled process at the anodic polarization ranged from 32 to 132 mV vs. open circuit potential (OCP). The rate constant of charge transfer for the anodic oxidation of V(IV) increases from 1.2×10^{-5} to 17.7×10^{-5} cm s^{-1} with temperature varied from 20 to 60 ^oC, and its activation energy is 52.4 kJ mol^{-1}.

Keywords: Vanadium redox flow battery, graphite electrode, impedance, kinetic parameter, activation energy

1. INTRODUCTION

The vanadium redox battery(VRB) is a type of rechargeable flow battery which employs vanadium redox couples due to the ability of vanadium to exist in solution in four different oxidation states [1, 2]. The redox couples of V(II)/V(III) and V(IV)/V(V) are employed as the negative and positive electrode reactions, respectively. It has been found that in previous work[3-5], the kinetics of the V(IV) to V(V) reaction are slower and more complex because vanadium ions in higher oxidation states trend to coordinate with oxygen ions in the electrolyte solution. In addition, the studies show that the performance and electrode reaction kinetics of the VRB, especially for the positive side, are dramatically influenced by temperature because the stability and solubility of V(V) species decrease with increasing temperature at the high concentration of V(V) species. F. Rahman studied the effect of

temperature on stability of the V(V) in the positive half-cell electrolyte[6]. Although many investigations have been conducted on the kinetics and reaction mechanisms of electrode process of the V(IV)/V(V) couple on different electrodes in the ambient environment[7-11], few works about the influence of temperature on the electrochemical behavior of V(IV)/V(V) couple can be found in the literature at present.

The objective of this work is to investigate the effect of temperature on the electrochemical characteristic of the anodic oxidation of V(IV) in 2 mol dm^{-3} H_2SO_4 solution by steady-state polarization and AC impedance measurements with DC bias, so as to estimate the kinetic parameters and the activation energy of the anodic oxidation of V(IV).

2. EXPERIMENTAL

2.1. Chemicals

The electrolyte in this study was a 2 mol dm^{-3} vanadyl sulfate ($VOSO_4$) solution, with the supporting electrolyte of 2 mol dm^{-3} sulfuric acid. All chemicals were of analytical grade and were used as received without any purification, and de-ionized water was used for all experimental solutions.

2.2. Fabrication of the working graphite electrodes

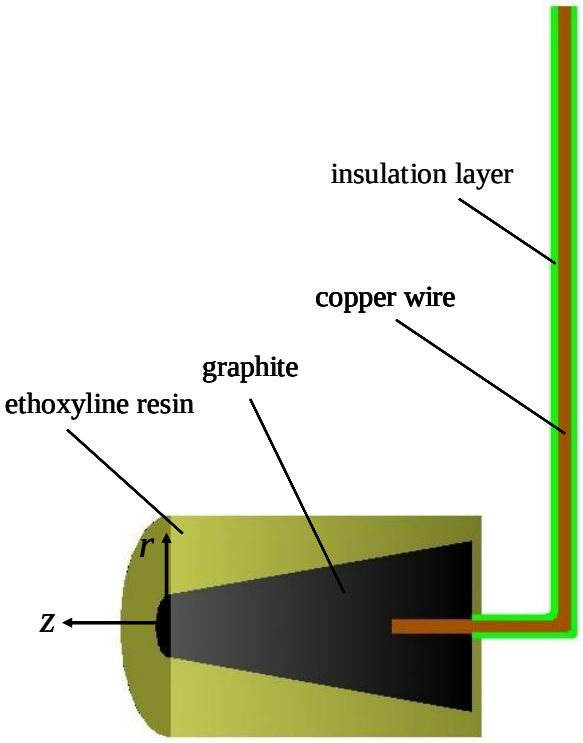

Figure 1. The schematic diagram of fabricating the graphite electrode

The graphite electrode was made of spectroscopically pure graphite rod with a radius of 5 mm, supplied by Sinosteel Shanghai Advanced Graphite Materials Company (China). The graphite rod was cut about 10 mm high with a tip of 1 mm in radius at its one end, and connected with a copper wire at the other end, then inlaid within an ethoxyline resin column. The schematic diagram of the prepared graphite electrode was shown in Figure 1. One of the key things for fabrication of the graphite electrode is to control the working surface with the desired dimension by abrading the graphite rod within the ethoxyline resin at the spiry end. While the open tip was near to 2.5 mm in radius, it was subsequently polished using SiC abrasive paper down to 2000 grit for about 5 min with the rotation rate of 300 rpm. Thereafter, it was subjected to ultrasonic cleaning in de-ionized water for 10 min to remove polishing residues, followed by air-dry. Finally, the working graphite electrode left a polished, circular disc with a radius of 2.5 mm exposed to the electrolyte.

2.3. Electrochemical measurements

All experiments were performed in a plexiglass cell containing with about 0.3 dm^{-3} of 2 mol dm^{-3} H_2SO_4+2 mol dm^{-3} $VOSO_4$ electrolyte by a PARSTAT 2273-potentiostat/ galvanostat/FRA. The cell was kept in a water bath; thereafter the experiments were performed at 15, 20, 30, 40, 50, 60, and 70 ^oC. A conventional three-electrode setup was utilized, in which the reference electrode was saturated calomel electrode(SCE), the counter electrode a graphite plate with the dimension of 50 mm×60 mm, and the working electrode a graphite electrode prepared as described in section 2.2. The steady-state polarization curves were measured at a scanning rate of 2 mV s^{-1} starting from 0 mV up to 480 mV vs. the open circuit potential (OCP). Electrochemical impedance spectroscopies (EIS) were conducted in a frequency range between 0.1 and 100 kHz with the AC amplitude of 10 mV, at different DC bias typically ranged from 32 to 132 mV vs. OCP. The impedance spectra were analyzed by using the ZSimpWin software. Each impedance test was repeated three times, and the average impedance values obtained were used to calculate kinetic parameters.

2.4. Kinetic consideration

2.4.1. Determination of diffusion coefficient

$$VO_2^+ + 2H^+ + e^- \underset{\text{charge}}{\overset{\text{discharge}}{\rightleftharpoons}} VO^{2+} + H_2O \qquad (2.1)$$

The equation (2.1) shows that the electrochemical reaction occurs on the positive electrode of the vanadium flow battery during charge and discharge process, respectively [1, 2]. The diffusion equation describes one-step reaction taking place at a finite disc electrode surface inlaid within an ethoxyline resin column can be written as,

$$\frac{1}{D}\frac{\partial C_{VO^{2+}}(z,r,t)}{\partial t} = \frac{\partial^2 C_{VO^{2+}}(z,r,t)}{\partial r^2} + \frac{1}{r}\frac{\partial C_{VO^{2+}}(z,r,t)}{\partial r} + \frac{\partial^2 C_{VO^{2+}}(z,r,t)}{\partial z^2} \qquad (2.2)$$

Where *r* and *z* are the coordinates in directions parallel and normal to the electrode base plane, respectively, *t* represents time, $C_{VO^{2+}}(z,r,t)$ is the concentration of species VO^{2+}, and *D* is the diffusion coefficient of species VO^{2+}.

When the system is in a steady state, the partial derivative of concentration with respective to time is zero,

$$\frac{\partial C_{VO^{2+}}(z,r,t)}{\partial t}=0 \qquad (2.3)$$

Then, the diffusion equation (2.2) can be substituted by equation (2.4),

$$\frac{\partial^2 C_{VO^{2+}}(z,r,t)}{\partial r^2}+\frac{1}{r}\frac{\partial C_{VO^{2+}}(z,r,t)}{\partial r}+\frac{\partial^2 C_{VO^{2+}}(z,r,t)}{\partial z^2}=0 \qquad (2.4)$$

To calculate the diffusion-limiting current to a finite disc electrode surface, equation (2.4) is solved with the flowing initial and boundary conditions,

Initial conditions to the inlaid disc electrode are,

$$t=0, C_{VO^{2+}}(z,r,0)=C^*_{VO^{2+}}; C_{VO_2^+}(z,r,0)=C^*_{VO_2^+}=0 \qquad (2.5)$$

and the boundary conditions are,

$$t>0, z=0, r\le r_0, C_{VO^{2+}}(z,r,t)=C^0_{VO^{2+}} \qquad (2.6)$$

$$t>0, z=0, r>r_0, \frac{\partial C_{VO^{2+}}(z,r,t)}{\partial z}=0 \qquad (2.7)$$

$$t>0, z\to\infty, C_{VO^{2+}}(z,r,t)=C^*_{VO^{2+}} \qquad (2.8)$$

$$t>0, r\to\infty, C_{VO^{2+}}(z,r,t)=C^*_{VO^{2+}} \qquad (2.9)$$

where $C^*_{VO^{2+}}$ is the bulk concentration of species VO^{2+}, $C^*_{VO_2^+}$ is the bulk concentration of species VO_2^+, $C^0_{VO^{2+}}$ the concentration of species VO^{2+} on the electrode surface, and r_0 the radius of the disc electrode.

Furthermore, the steady-state limiting current on the finite disk electrode surface can be obtained by assuming the concentration of $C^0_{VO^{2+}}$ on the electrode surface is zero [12, 13],

$$i_L=4nFDC^*_{VO^{2+}}r_0 \qquad (2.10)$$

where i_L is the limiting current, F the Faraday constant, n is the number of electrons transferred in the redox reaction shown in equation (2.1). Therefore, the diffusion coefficient can be calculated from the equation (2.10).

2.4.2. Determination of activation energy

The kinetics of the electron transfer at the interface between the graphite electrode and electrolyte was analyzed according to the Bulter-Volmer equation. The current density can be expressed as equation (2.11).

$$i = Fk_s[C^0_{VO_2^+} \exp(-\frac{\alpha F\eta}{RT}) - C^0_{VO^{2+}} \exp(\frac{(1-\alpha)F\eta}{RT})] \qquad (2.11)$$

Where k_s is the standard rate constant, α the energy transfer coefficient, η the overpotential, $C^0_{VO_2^+}$ the concentration of VO_2^+ on the electrode surface. Other symbols in the equation have their usual electrochemical significance. Under the experimental conditions used in this work, the concentration of $C^0_{VO^{2+}}$ is 2 mol dm^{-3} while $C^0_{VO_2^+}$ is near to zero at the beginning of anodic polarization. The AC impedance measurements were carried out under the Direct-Current (DC) anodic polarization, which ranged from 32 to 132 mV vs. OCP, so the cathodic current for reduction of VO^{2+} may be neglected. Furthermore, the electrode process should be characterized as the faradic charge-transfer behavior, when the Nyquist impedance plot shows the semi-circle at high frequencies. Then, the $C^0_{VO^{2+}}$ can be used of the bulk concentration of $C^*_{VO^{2+}}$, Thereafter, the equation (2.11) can be simplified to the equation (2.12).

$$i = -Fk_s[C^*_{VO^{2+}} \exp(\frac{\beta F\eta}{RT})] \qquad (2.12)$$

Where β=1-α. By differentiation of η with respect to i, Equation (2.13) is obtained:

$$(-\frac{d\eta}{di})_{\eta\neq 0} = -\frac{RT}{\beta Fi} \qquad (2.13)$$

The value of $[-d\eta / d(i)]_{\eta\neq 0}$ in equation (2.13) is equal to the faraday impedance, R_{ct}, which can be obtained from the diameter of the semicircle of the Nyquist impedance plot. Combining equation (2.13) and (2.12) and substituting R_{ct} for $[-d\eta / d(i)]_{\eta\neq 0}$, the relationship of η and R_{ct} can be shown as equation (2.14).

$$\eta = \frac{2.3RT}{\beta F}\log\frac{1}{R_{ct}} + \frac{2.3RT}{\beta F}\log\frac{RT}{\beta F^2 k_s C^*_{VO^{2+}}} \qquad (2.14)$$

$R_{ct,0}$, $[-d\eta/d(i)]_{\eta=0}$ can be obtained by extending the linear region of the plot to $\eta = 0$. The slope of the linear plot can yield the value of the energy-transfer coefficient and the intercept can give the standard rate constant, k_s[14]. The temperature dependence of the standard rate constant, k_s also can be determined by the relationship of η and R_{ct} at varied temperatures. According to equation (2.15), the activation energy of charge transfer without any DC polarization potential can be evaluated.

$$\ln k_s(T) = \ln A - \frac{E_a}{RT} \qquad (2.15)$$

Where $k_s(T)$ is the standard rate constant at the temperature (T), A the frequency factor, and E_a the activation energy for charge transfer of the electrochemical oxidation of VO^{2+}.

3. RESULTS AND DISCUSSION

3.1. steady-state polarization study for V(IV)/V(V) redox at various temperatures

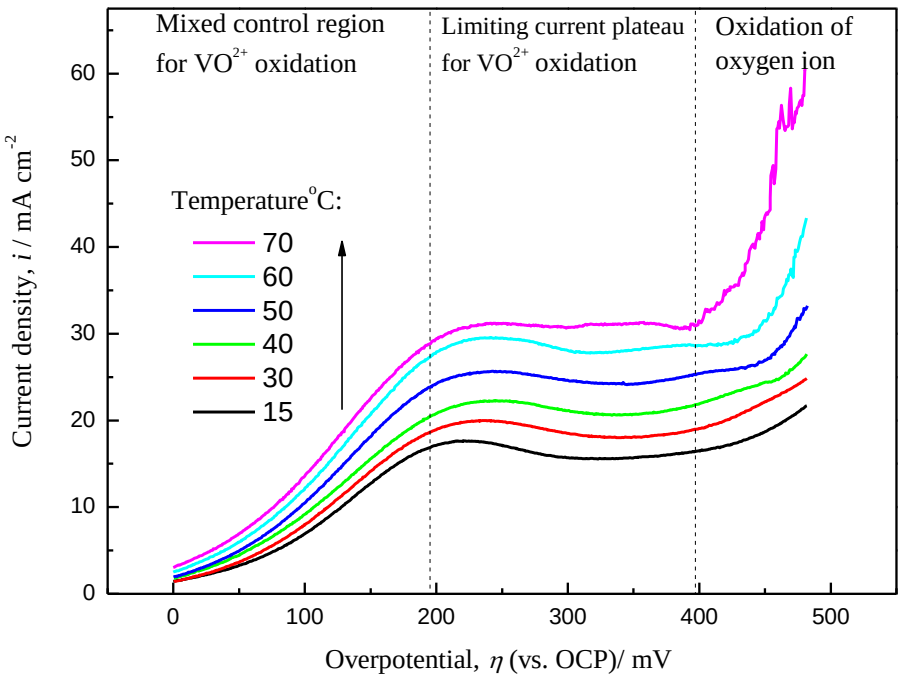

Figure 2. Steady-state polarization curves of the graphite electrode in 2 mol dm^{-3} H_2SO_4+2 mol dm^{-3} $VOSO_4$ solution at different temperatures; scan rate: 2 mV s^{-1}

The steady-state polarization curves of graphite electrode in 2 mol dm^{-3} H_2SO_4 + 2 mol dm^{-3} $VOSO_4$ solution at different temperatures are shown in Figure 2. The curves show three zones: the first linear region corresponds to the mixed control process, where the primary reaction, electrochemical oxidation of VO^{2+}, is controlled by both mass transport and electron transfer; then the plateau region

to the complete mass transport control; finally, the final polarized section to the processes, where the secondary reaction (oxidation of oxygen ion) occurs besides the primary reaction[15]. As the temperature increasing from 15 to 70 ^{o}C, the current density within the mixed control region increases, which is due to the enhancements of the VO^{2+} diffusion and its oxidation. Meanwhile, the limiting current density in the plateau region is also increases from 15.8 to 31.0 mA cm^{-2}. The presence of the limiting current density for the plateau region indicates that the transport of VO^{2+} ions to the surface of the electrode is the controlling step when the overpotential of the anode is more than 250 mV. Furthermore, the diffusion rate of VO^{2+} ions increases with temperature. Therefore, the diffusion coefficients can be calculated from the equation (2.10) at the different temperatures when other parameters are known, which are presented in Table 1.

Table 1. The diffusion coefficient of V(IV) species in 2 mol dm^{-3} H_2SO_4 at different temperatures

Solution temperature / ^{o}C	Diffusion coefficient, $D\times10^{5}$ /cm^{2} s^{-1}
15	1.60
30	1.86
40	2.13
50	2.49
60	2.86
70	3.15

The effect of temperature on the diffusion of VO^{2+} ion in 2 mol dm^{-3} H_2SO_4+2 mol dm^{-3} $VOSO_4$ solution was investigated at the varied temperature between 15 and 70 ^{o}C. The diffusion activation energy, E_d was evaluated by the Arrhenius equation (3.1),

$$D(T) = D_0 \exp(-\frac{E_d}{RT}) \qquad (3.1)$$

Where D_0 is the temperature-independent factor (cm^2 s^{-1}), E_d the diffusion activation energy (kJ mol^{-1}), R the gas constant and T the solution temperature(K). According to the data in Table 1, a plot of ln$D$ vs. 1/T can be obtained in Figure 3, which illustrates an excellent correlation of the data to the Arrhenius relationship. Therefore, the activation energy for diffusion of V(IV) species is 10.52 kJ mol^{-1}. There have been several researches on the diffusion coefficient of V(IV) by electrochemical methods, which are shown in Table 2 with the result of this work. Although the diffusion coefficient in the electrolyte is independent of the electrode material, it shows that the surface geometry of electrode seems to be crucial for high precision evaluation of diffusion coefficients with considering the additional influence of the species concentration. For the kind of carbon electrodes with relatively smooth surface, such as a glassy carbon or pyrolytic graphite electrode, the evaluated diffusion coefficient is smaller compared with that of the electrode with less smooth surface, e.g. graphite felt,

carbon paper or graphite disc electrode. Maybe the later one has larger real surface area than its projective area, which makes the evaluated diffusion coefficient larger than its true value.

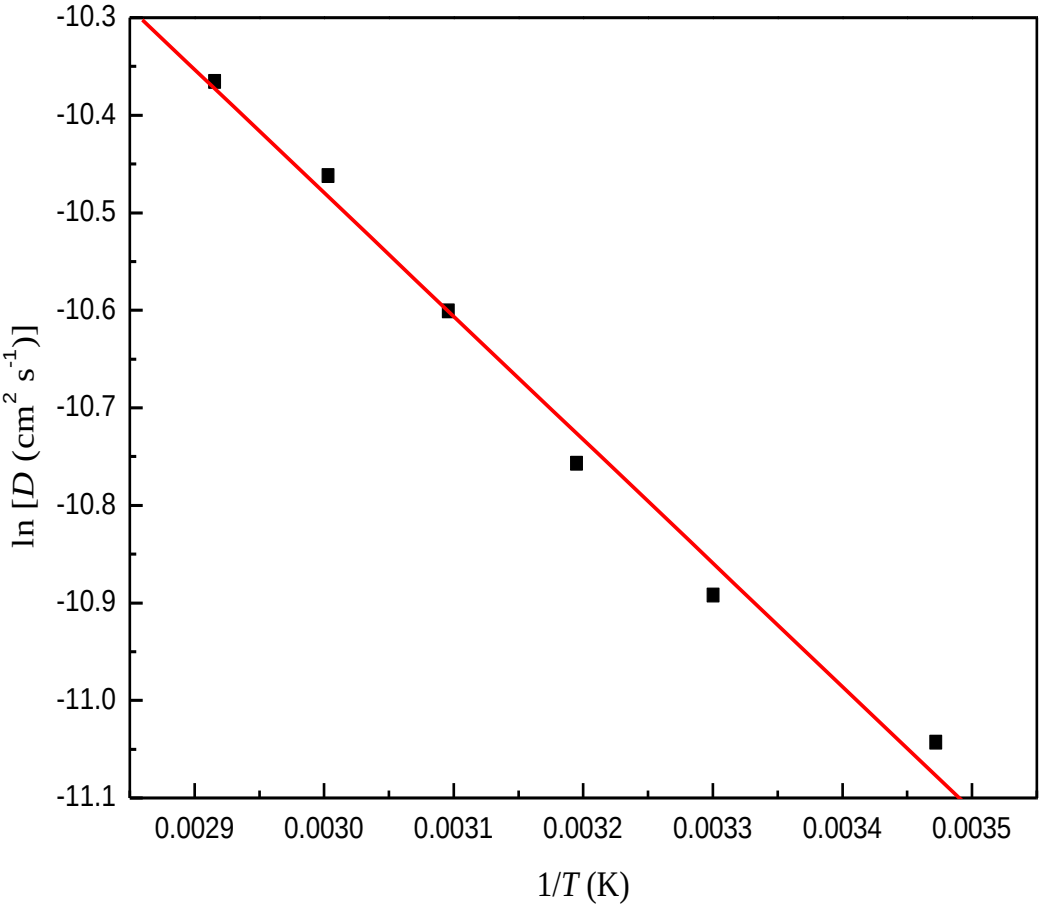

Figure 3. The plot of ln*D* versus 1/*T* for the anodic oxidation of V(IV) on the graphite electrode in 2 mol dm^{-3} H_2SO_4+2 mol dm^{-3} $VOSO_4$ solution.

It is very difficult to determine the accurate real area of the electrode because of its unknown surface micro-roughness and wettability to the electrolyte. However, the magnitude of the diffusion coefficient of V(IV) varies from 10^{-5} to 10^{-6} cm^2 s^{-1} by using the different kinds of carbon electrodes, which is probably acceptable. It is possible to neglect the 'false surface area' effect when the activation energy for diffusion was determined in this study by comparing the limiting current density values at various temperatures, since the real working surface of the graphite electrode should keep almost constant at varied temperature from 15 to 70 ^oC, and can be eliminated in the expressions during evaluation.

In addition, the section of the steady-state polarization plots for the secondary electrochemical reaction in Figure 2 shows the overpotential required for oxidation of oxygen ion decreases as temperature increasing. Furthermore, the slop of the current density versus overpotential increases with increased temperature. It indicates high temperature can enhance oxygen ion oxidation at the anode, which can lead to deterioration of graphite electrodes on the positive side.

Table 2. The diffusion coefficient of V(IV) species reported in some literature and the result of this work

Electrode	T / °C	$C_{H_2SO_4}$ / mol dm^{-3}	$C_{VO^{2+}}$ / mol dm^{-3}	$D \times 10^5$ / cm^2 s^{-1}	Method	Sources
graphite	Room temperature	3	0.5	0.186	Cyclic and rotating-disc voltammetry	[4]
glassy carbon	Room temperature	2	2	0.0889	Rotating-disc voltammetry	[5]
graphite	20	1	0.09	0.20	Polarization curve	[10]
graphite felt	22	1.6	1	4.4	Cyclic voltammetry	[16]
graphite	Room temperature	1.9	0.033	0.30	Polarization curve	[17]
carbon paper	Room temperature	3	0.8	4.5	Polarization curve	[18]
glassy carbon	Room temperature	5	0.035	0.10	Cyclic voltammetry	[19]
plastic formed carbon	25	1	0.05	0.39	Cyclic voltammetry	[20]
glassy carbon	25	1	0.05	0.28	Cyclic voltammetry	[20]
pyrolytic graphite	25	1	0.05	0.24	Cyclic voltammetry	[20]
graphite	15	2	2	1.6	Polarization curve	This work

3.2 Electrochemical impedance spectroscopy

The Nyquist plots of the graphite electrode in 2 mol dm^{-3} H_2SO_4+2 mol dm^{-3} $VOSO_4$ solution at different temperatures under various DC bias are shown in Figure 4. The plots show that, in the high frequency region, the experimental curves have the shape of a semi-circle, whereas it is a straight line with a slope of unity approximately in the low frequency region. It indicates the anodic oxidation of V(IV) on graphite electrode is a mixed kinetic-diffusion controlled process in 2 mol dm^{-3} H_2SO_4+2 mol dm^{-3} $VOSO_4$ solution at different DC bias typically ranged from 32 to 132 mV vs. OCP. The experimental data are accurately fitted by the equivalent circuit of the AC impedance diagram shown in Figure 4 (f), where R_s stands for the resistance of solution from the nozzle of Luggin capillary to working electrode surface, Q the constant phase element (CPE), R_{ct} the charge transfer resistance and W the Warburg diffusion impedance.

The equivalent circuit simulation for graphite electrode at different temperatures under various DC bias are shown in Table 3a and Table 3b. The slope of the straight line deviating from unity in the

lower frequency range of the Nyquist plots may be explained by the roughness of the electrode surface or the shallow pores on the surface of the electrode [22].

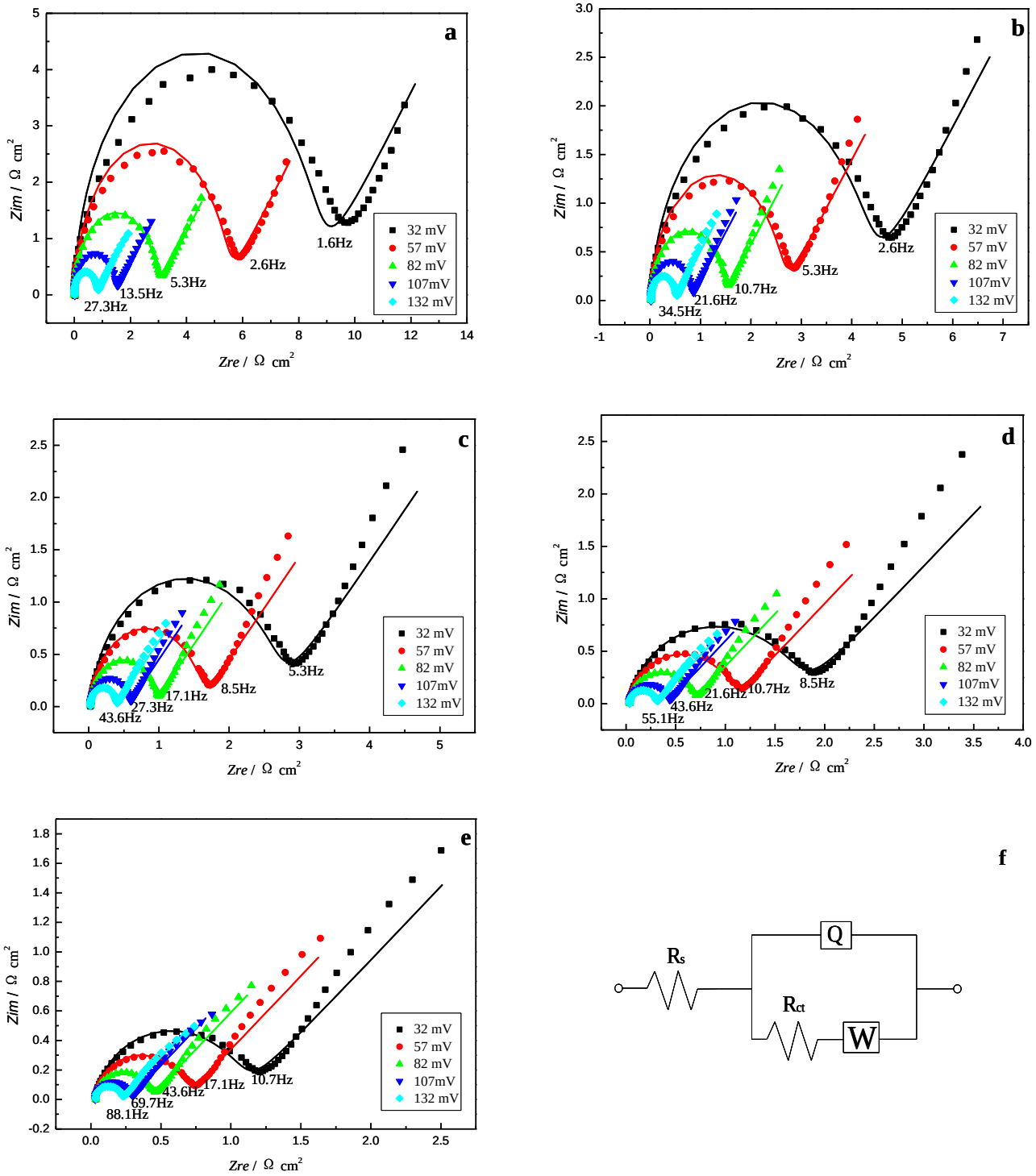

Figure 4. Nyquist plots of the graphite electrode in 2 mol dm^{-3} H_2SO_4+2 mol dm^{-3} $VOSO_4$ solution at different temperatures(a:20 °C, b:30 °C, c:40 °C, d:50 °C, and e:60 °C) and under various DC bias(■:32 mV, ●: 57 mV, ▲: 82 mV, ▼: 107 mV, ◆:132 mV), where the point symbols are experimental points and the solid lines are the fitted lines, and f: Equivalent circuit for the AC impedance.

Table 3a The equivalent circuit simulation of R_{ct} for graphite electrode in 2 mol dm^{-3} H_2SO_4+2 mol dm^{-3} $VOSO_4$ solution at different temperatures under various DC bias.

DC bias / mV	R_{ct} / Ω cm^2				
	20 °C	30 °C	40 °C	50 °C	60 °C
32	7.46	3.89	2.46	1.60	0.98
57	4.36	2.25	1.45	0.96	0.61
82	2.30	1.24	0.83	0.58	0.38
107	1.16	0.70	0.49	0.35	0.24
132	0.65	0.42	0.32	0.24	0.18

Table 3b The equivalent circuit simulation of Warburg impedance coefficient of the graphite electrode in 2 mol dm^{-3} H_2SO_4+2 mol dm^{-3} $VOSO_4$ solution at different temperatures under various DC bias.

DC bias / mV	Warburg impedance coefficient, σ / Ω $cm^2 \cdot s^{-0.5}$				
	20 °C	30 °C	40 °C	50 °C	60 °C
32	4.04	2.82	2.35	2.02	1.57
57	2.57	1.88	1.57	1.35	1.09
82	1.88	1.35	1.13	0.97	0.78
107	1.41	1.01	0.86	0.76	0.61
132	1.18	0.88	0.78	0.66	0.52

The semi-circle at the high frequency is due to the combination of the double layer capacitance, and the charge transfer reaction at the electrolyte/electrode interface which was associated with oxidation of V(IV) ions. The decrease of the charge transfer resistance R_{ct} with the overpotential increasing can be explained based on the equation (2.14), which shows log R_{ct} versus η behavior. The plots of η versus $\log(1/R_{ct})$ at different temperatures under the applied overpotentials are shown in Figure 5.

According to Eq. (2.14), the values of $R_{ct,0}$, i_0, and k_s are evaluated and shown in Table 4. The charge transfer resistance $R_{ct,0}$ decreases with temperature increasing. The exchange current density i_0 increases from 2.4×10^{-3} to 34.2×10^{-3} A cm^{-2}, and the standard rate constant k_s from 1.2×10^{-5} to 17.7×10^{-5} cm s^{-1}, with temperature elevated from 20 to 60 °C. It can be deduced that the anodic oxidation of V(IV) on graphite electrode proceeds faster at higher temperature. The plot of $\ln k_s$ versus $1/T$ for the anodic oxidation of V(IV) on graphite electrode in 2 mol dm^{-3} H_2SO_4+2 mol dm^{-3} $VOSO_4$ solution is shown in Figure 6, which illuminates the Arrhenius-type temperature dependence of the rate constant k_s. The charge transfer activation energy (E_a) for oxidation of V(IV) is evaluated as 52.4 kJ mol^{-1}.

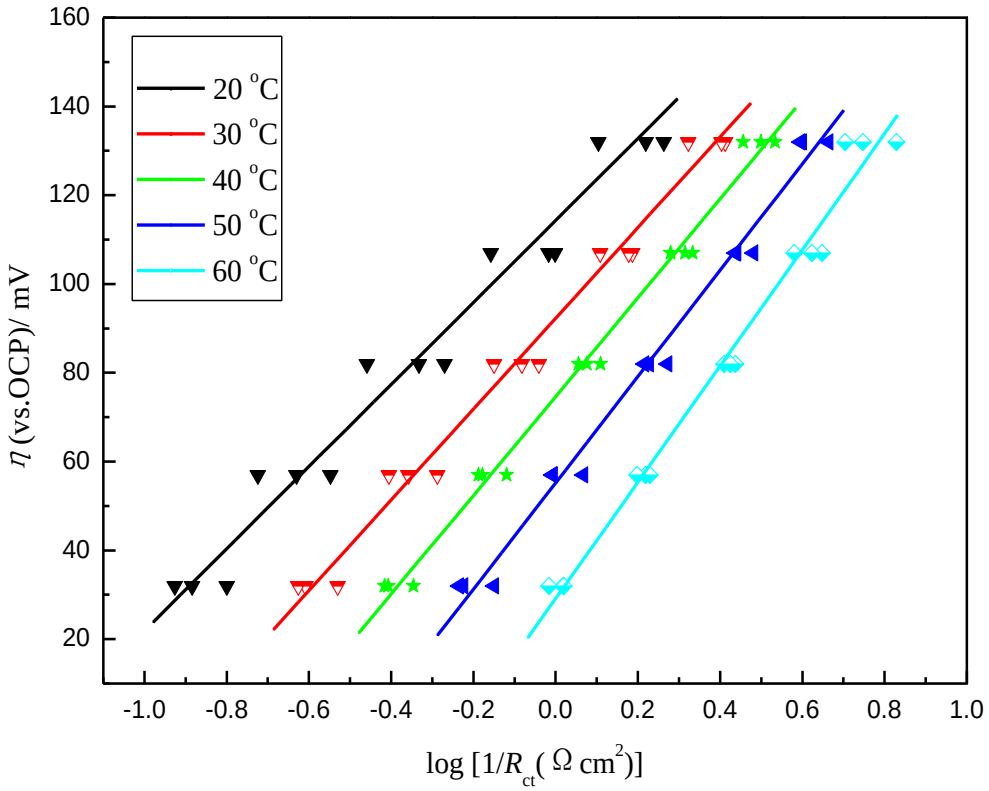

Figure 5. Plots of η (vs.OCP) versus $\log(1/R_{ct})$ at different temperatures under the applied overpotentials, where the point symbols are experimental points and the solid lines are the fitted lines.

Table 4. The values of kinetic parameters (i.e., anodic transfer coefficient β, charge transfer resistance $R_{ct,0}$, exchange current density i_0, rate constant k_s) and correlation coefficients R obtained at different temperatures for the anodic oxidation of V(IV) on the graphite electrode in 2 mol dm^{-3} H_2SO_4+2 mol dm^{-3} $VOSO_4$ solution.

Temperature / °C	β	$R_{ct,0}$ / *Ω cm²*	$i_0 \times 10^3$ / *A cm⁻²*	$k_s \times 10^5$ / *cm s⁻¹*	*R*
20	0.63	17.4	2.4	1.2	0.9989
30	0.59	8.0	5.7	2.9	0.9995
40	0.56	4.7	10.5	5.4	0.9989
50	0.53	2.9	18.2	9.4	0.9985
60	0.51	1.7	34.2	17.7	0.9968

The value of the Warburg impedance coefficients are shown in Table 3b for the varied DC bias at different temperatures resulting from the equivalent electrical circuit used for fitting the EIS data, presented in Fig4. The results show that the Warburg impedance coefficient decreases with increasing temperature and DC bias, probably because it contains some information about V(IV) diffusion in the electrolyte and surface character of the electrode. However, the DC bias dependence of the Warburg impedance is currently not well understood.

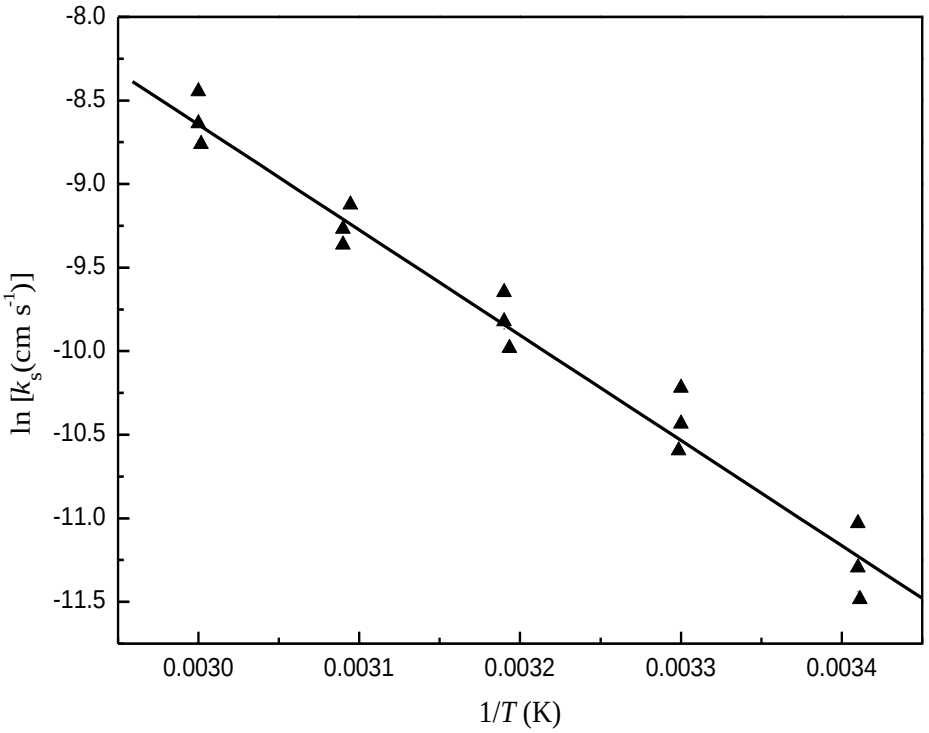

Figure 6. The plot of lnk_s versus 1/T for the anodic oxidation of V(IV) on graphite electrode in 2 mol dm^{-3} H_2SO_4+2 mol dm^{-3} $VOSO_4$ solution.

4. CONCLUSIONS

The effect of temperature on the electrochemical behavior of the anodic oxidation of V(IV) in 2 mol dm^{-3} H_2SO_4+2 mol dm^{-3} $VOSO_4$ solution was studied with the graphite electrode by steady-state polarization and AC impedance measurements. The results show that the anodic oxidation of V(IV) is a mixed kinetic-diffusion controlled process. The diffusion coefficient (D) of V(IV) species is increased with increasing temperature and the activation energy for diffusion of V(IV) species was 10.52 kJ mol^{-1}. Both the exchange current density i_0 and rate constant k_s increased with increasing temperature from 20 to 60 ^{o}C, which means the reaction rate of the anodic oxidation of V(IV) is faster at higher temperature. The activation energy for charge transfer of the anodic oxidation of V(IV) is 52.4 kJ mol^{-1}evaluated at the temperature varied from 20 to 60 ^{o}C.

ACKNOWLEDGMENTS
The authors acknowledge the financial support of Natural Science Foundation of Liaoning province, China (Grant No.99106003) and the financial support of the Fundamental Research Funds for the Central Universities (Grant No. N100602009).

References

1. E. Sum, M. Rychcik and M. Skyllas-Kazacos, *J. Power Sources*, 16 (1985) 85

2. E. Sum and M. Skyllas-Kazacos, *J. Power Sources*, 15 (1985) 179
3. M. Gattrell, J. Qian, C. Stewart, P. Graham and B. MacDougall, *Electrochim. Acta*, 51 (2005) 395
4. S. Zhong and M. Skyllas-Kazacos, *J. Power Sources*, 39 (1992) 1
5. Y.H. Wen, H.M. Zhang, P. Qian, H.P. Ma, B.L. Yi and Y.S. Yang, *Chin. J. Chem*., 25 (2007) 278
6. F. Rahman and M. Skyllas-Kazacos, *J. Power Sources*, 189 (2009) 1212
7. Y.H. Wen, H.M. Zhang, P. Qian, P. Zhao, H.T. Zhou and B.L. Yi, Acta. *Phys.-Chim. Sin*., 22 (2006) 403
8. G. Oriji, Y. Katayama and T. Miura, *Electrochim. Acta*, 49 (2004) 3091
9. H. Kaneko, K. Nozaki, Y. Wada, T. Aoki, A. Negishi and M. Kamimoto, *Electrochim. Acta*, 36 (1991) 1191
10. M. Gattrell, J. Park, B. MacDougall, J. Apte, S. McCarthy and C.W. Wu, *J. Electrochem. Soc*., 151 (2004) A123
11. H.Q. Zhu, Y.M. Zhang, L. Yue, W.S. Li, G.L. Li, D. Shu and H.Y. Chen, *J. Power Sources*, 184 (2008) 637
12. Bala´zs Cso´ka and Ge´za Nagy, *J. Biochem. Biophys. Methods*, 61 (2004) 57
13. C.G. Zoski and Mirkin, M.V. *Anal. Chem*., 74 (2002) 1986
14. P. Elumalai, H.N. Vasan and N. Munichandraiah, *J. Solid State Electrochem*., 3 (1999) 470
15. H. Al-Fetlawi, A.A. Shah and F.C. Walsh, *Electrochim. Acta*, 55 (2010) 3192
16. X.G. Li, K.L. Huang, S.Q. Liu and L.Q. Chen, *J. Cent. South Univ*. T., 14 (2007) 51
17. M. Gattrell, J. Qian, C. Stewart, P. Graham and B. MacDougall, *Electrochim. Acta*, 51 (2005) 395
18. S.Q. Liu, X.H. Shi, K.L. Huang, X.G. Li, Y.J. Li and X.W. Wu, Chinese *J. Inorg. Chem*., 25 (2009) 417
19. G. Oriji, Y. Katayama and T. Miura, *J. Power Sources*, 139 (2005) 321
20. T. Yamamura, N. Watanabe, T. Yano and Y. Shiokawa, *J. Electrochem. Soc*., 152 (2005) A830
21. S.A.G.R. Karunathilaka and N.A. Hampson, *J. Appl. Electrochem*., 11 (1981)365